FULL PAPER
THE ANALYST
www.rsc.org/analyst

Analysis of luminescence spectra of leucite ($KAlSiO_4$)

Javier Garcia-Guinea,[a] Virgilio Correcher*[b] and Eduardo Rodriguez-Badiola[a]

[a] *Museo Nacional de Ciencias Naturales, C/José Gutiérrez Abascal 2, Madrid 28006, Spain*
[b] *CIEMAT, Ed. 2, Av. Complutense 22, Madrid 28040, Spain. E-mail: v.correcher@ciemat.es*

Received 27th February 2001, Accepted 29th March 2001
First published as an Advance Article on the web 8th May 2001

High-sensitivity radioluminescence (RL) and thermoluminescence (TL) measurements were carried out on samples of natural leucite (with 2.95% of Na_2O) from Campania Vessa (Italy). Samples were annealed to modify the charge compensation through alkali metal self-diffusion and to produce luminescence centres. High-temperature powder diffraction, scanning electron microscopy and chemical analyses were performed to monitor the tetragonal–cubic phase transitions and the thermal drainage of alkali metal ions from the aluminosilicate lattice. The emission spectral bands of leucite (300, 380, 430, 480, 560 and 680 nm) match those of other Na/K-aluminosilicates (alkali metal feldspars) and could be attributed to similar defects. TL glow curves of increasingly pre-irradiated natural leucite (range 0–20 Gy) showed no changes above 300 °C, whereas some changes were observed with annealed samples (1000 °C for 12 h). This temperature is the starting point of Na self-diffusion within the aluminosilicate lattices. The areas of the TL glow curves of both natural and annealed β-irradiated leucites can be fitted with a linear function with high correlation. These results are in agreement with high alkali metal loss (K_2O ~12% and Na_2O ~18%) during thermal pre-treatment, high cell volume expansion (from 2350 to 2500 Å) and the cubic $Ia3d \rightleftharpoons$ tetragonal $I4_1/a$ phase transition. This promotes the egress of alkali metal ions and the production of $[AlO_4/M^+]°$, $[AlO_4/H^+]°$ and $[AlO_4]°$ luminescence centres.

Introduction

Leucite ($KAlSiO_4$) is used in the manufacture of glasses[1] and porcelains as one of the main components employed in ceramics for dental restoration.[2,3] In the most common procedure to prepare dental porcelains, a thermal treatment at 930 °C is required. The main interest in the use of this feldspathoid is the lower specific gravity (<2.5) in comparison with feldspars (>2.5) and its structure permits the substitution of large cations, because of the larger hollow space in four- and six-membered SiO_4 rings. Large anions can be hosted in these cavities and coordinated to oxygen in the enclosing rings. Simply considering albite–anorthite solid solution and taking out one SiO_2 derives the formula for leucite. It is known that quartz and Na- and K-aluminosilicates (albite and microcline, respectively) found in other ceramic materials (tiles, bricks, glazed basins, *etc.*) can be used in the field of geological and archaeological dating and retrospective dosimetry that have analytical routines based on luminescence methods (blue emissions around the 400 nm). Aluminosilicate lattices are formed by SiO_4 tetrahedra with interlinked corners. If no ion substitutes the Si, the whole framework is SiO_2 and all valence bonds are satisfied. When Al substitutes the Si in the tetrahedra, interstitial cations (Li^+, Na^+, K^+, Ca^{2+}) are required to preserve charge balance.

The role of $[AlO_4]°$ centres in the blue thermoluminescence of quartz was described by Martini *et al.*,[4] who also demonstrated that prolonged high-temperature annealing of the samples reduces the presence of ionic charge compensators and creates luminescence traps. The equivalent effect is observed when feldspars are pre-heated, increasing the sensitisation of the blue broad band, *e.g.*, the new type of regenerated thermoluminescence (TL) in an albite.[5] Also for feldspathoids (leucite, sodalite or nepheline), annealing of its anhydrous framework silicates improves the TL sensitivity of natural minerals.[6,7]

The intrinsic organisation of feldspar and feldspathoid parastructures includes twinning planes, antiphase domain boundaries, exsolution borders, modulations, *etc*. These natural superlattice complexities give many different points of egress for the alkali metal ions during thermal treatments; many distinct sets of dynamic TL traps are produced which could explain the difficulty in parameterising the TL glow curves of alkali metal aluminosilicates.

Leucite crystals from volcanic lava flows were selected because they offer an interesting property linked with the thermal leakage of alkali metal ions: a phase transition at low temperature (~650 °C). These natural crystals show polysynthetic (pseudomerohedric) twinning on {110} of the cubic phase, which is lost during the phase transition. At room temperature, leucite is tetragonal (space group $I4_1/a$) and contains an aluminosilicate framework of rings of SiO_4 and AlO_4 tetrahedra and displays cubic topological symmetry.[8] Leucite turns metrically cubic above ~665 °C (space group $Ia3d$). An intermediate tetragonal phase with space group $I4_1/acd$ is stable over the range 645–665 °C.[9] Palmer *et al*.[9] explained that the structural transition is too rapid to be caused by Al–Si ordering and that the primary instability is due to a displacive mechanism independent of any Al–Si ordering. They proposed that it is possible to produce disordered configurations that have no Al–O–Al linkages (driving force for ordering) owing to the relatively high ratio (2:1) of Si to Al atoms in the leucite lattice. High-temperature electron microscope experiments indicated that on annealing, the merohedric twins dissolve first, followed by polysynthetic twinning.[10] In terms of Landau theory, the Al/Si order is considered as a primary order parameter to which K^+ ion displacements couple linearly. K^+ ions move closer to oxygen atoms shared by Al and Si and away from those shared by two Si atoms. In addition, the small Na^+ ions move more easily through the leucite lattice producing $[AlO_4/M^+]°$, $[AlO_4/H^+]°$ and $[AlO_4]°$ luminescence centres.

Using the high-sensitivity spectrometer at the University of Sussex (UK) (radioluminescence, RL), the emission bands of leucite (wavelength *vs.* intensity) from 200 to 800 nm were measured. In addition, the sensitivity and the dose dependence of leucite under different exposures to β-radiation were studied using 2D-TL spectra (temperature *vs.* intensity). The investigation of the luminescence of leucite and the high-temperature monitoring of phase transitions is a key to understanding the

thermal leakage of alkali metal ions from aluminosilicate lattices.

Experimental

Measurements were carried out using natural white and clean leucite samples from Campania Vessa (Italy). Sample number LEU-IT-30 was selected from a set of well-characterised leucites from the mineral collection of the Museo Nacional de Ciencias Naturales (Madrid, Spain). Scanning electron microscopy (SEM) observations were made using a Zeiss DSM-90 (40 kV electron microscope with a resolution of 70 Å). The microanalysis detector was an Si–Li model, using a Tracor Northern Z2 computer. Sample metallizations were made using gold vapour in a vacuum (50 Å gold cover). Bulk analyses were carried out by atomic absorption spectrometry using a Perkin-Elmer Model 2380 and by X-ray fluorescence using a Philips PW1410 spectrometer with an Sc–Mo tube (Si, Al, Ti, Fe, Mg, Mn, Ca, Na and K elements). Samples of 0.3 and 5.5 g of anhydrous lithium tetraborate were prepared as glass discs melted in a platinum crucible. For this purpose a PERL'X2 was used.

The leucite lattices at room temperature were tested by X-ray diffraction using a Siemens D-5000 automated diffractometer with Cu Kα radiation. The patterns were obtained by step scanning from 2 to 64° 2θ in steps of 0.020° with a count of 6 s per step. High-temperature X-ray diffraction studies were performed in an Anton Paar chamber mounted on a Philips PW-1710 diffractometer. Samples were deposited on a platinum sheet. The temperature was recorded using a Pt–13% Rh/Pt thermocouple. All experiments were carried out in an air atmosphere.

Thermal treatments were carried out in a programmable temperature controlled tubular oven with a quartz chamber in open air. Heated samples were cooled to room temperature at 1 °C min^{-1}. Sample processing and measurements were carried out under red light.

Spectral measurements of natural and annealed LEU-IT-30 samples were made using the Sussex 3D TL spectrometer.[11] Signals were recorded over the wavelength range 200–800 nm, with a resolution of 5 nm for 100 point spectra and 3 nm for 200 point spectra, and all signals were corrected for the spectral response of the system. The RL was obtained during excitation and then samples were heated to 400 °C at 2.5 °C s^{-1} while the TL spectra were recorded. The X-ray unit tube was a Phillips MG MCN 101 X-ray tube with a current of 5 mA and a voltage of 5 kV delivering a dose rate of 10 Gy min^{-1} to the sample. The experimental spectral data of the RL analyses were fitted with multiparameter Gaussian functions using the Peak Fit program (supplied by Jandel Scientific Software). All the parameters were refined to a confidence limit of 95% accuracy.

More rigorous testing was carried out to clarify the effects of β-source exposure on the TL of the natural and pre-heated leucites. TL measurements were obtained using an automated Risø model TL DA-12 TL system developed by Risø National Laboratory.[12] This reader is provided with an irradiator unit containing a β-source of $^{90}Sr/Y$ with a dose rate of 27 mGy s^{-1} and an EMI 9635QA photomultiplier tube, and the emission was observed through a blue filter (FIB002) where the wavelength is peaked at 400 + 25, − 0 nm; the FWHM is 80 ± 16 nm and the peak transmittance (minimum) is 60%. The measurements were carried out using a linear heating rate of 5 °C s^{-1} up to 550 °C in an N_2 atmosphere. The leucite aliquots used (5.0 ± 0.1 mg each) were powdered with an agate pestle and mortar.

Results and discussion

Composition and structure

Externally, leucites show perfect trapezohedral crystals of size up to 3 cm. However, in section, they display some zoning of colour and polysynthetic twinning under a polarising microscope [(Fig. 1(a)]. Under SEM the leucite masses display a set of parallel fissures, which are linked with the polysynthetic twinning [Fig. 1(b)]. In other mixed leucite samples from Campania Vessa, mineral inclusions (pyroxene, olivine, plagioclase, *etc*.) and the boundary with the basaltic lava flow can be appreciated under both microscopes.

The chemical composition of the bulk natural sample LEU-IT-30 is displayed in Table 1. The sample shows a low analcimization grade, which is a natural alteration with an increase in Na content and decreases in K, Ca and Mg; the total iron content is constant, but Fe^{2+} increases (analcimization processes are linked to rapid cooling of the host basaltic lava flow). These natural Italian leucites were pre-heated at 1000 °C for 12 h and at 1200 °C for 240 h, leaking different amounts of alkali metal ions (K^+ and Na^+) from the aluminosilicate structure to create defects for further luminescence measurements. The most significant alkali metal losses are produced during the first thermal step (1000 °C for 12 h). During this step, K_2O decreases from 14.50 to 12.72%. However, during the second step (1200 °C for 240 h) it only decreases from 12.72 to 12.47%. The behaviour of the Na^+ losses is different, the leucite lattice leaks ~18% of Na^+ during the first annealing and ~23% during the second step at 1200 °C. (Table 1).

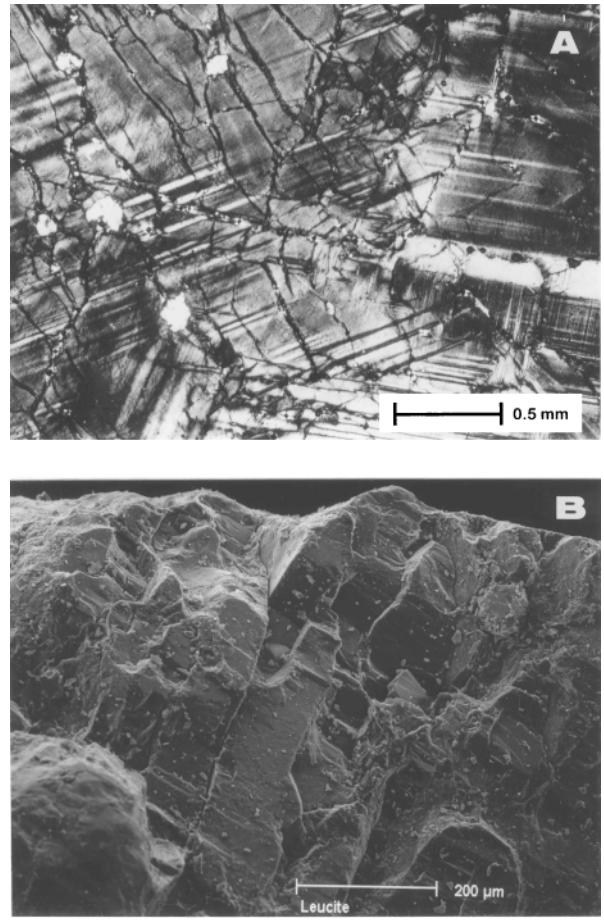

Fig. 1 Natural leucite (×300) from a basaltic lava flow (Campania Vessa, Italy). (A) Polarizing microscope image, twinning, and (B) scanning electron micrograph showing a set of parallel microfissures.

High-temperature powder X-ray diffraction patterns were recorded between room temperature and 800 °C. The set temperatures were independently calibrated by a secondary Pt–13% Rh/Pt thermocouple placed in the same position. Diffraction patterns were collected under isothermal conditions at varying intervals at 20, 500, 600, 650, 690, 800 and 20 °C after heating. The scan time was 33.5 min and the waiting time 10 min [Fig. 2(a)]. The temperature evolution of the (004) and (400) peaks reveals the first-order nature of the phase transition showing co-existing tetragonal and cubic peaks [Fig. 2(b)]. Twenty-six Bragg peaks (from 20 to 55° 2θ) were measured for cell-parameter determination using the least-squares refinement method with maximum deviations between observed and calculated values $\leqslant$0.003° 2θ. The cell volumes of the Campania Vessa leucite fit very well the relation between volume and temperature for leucite[13] [Fig. 2(c)]. The thermal evolution of (004) and (400) peaks is not uniform, denoting some anisotropies during the phase transition. Taylor and Henderson[14] explained the transformation (between 600 and 750 °C) as induced by the progressive breakdown of the tetrahedral lattice around the hollow containing the K^+ cation. The differences between the diffraction patterns at the original room temperature and room temperature after heating [Fig. 2(b)] can be explained by the transformation from the cubic space group *Ia*3*d* to the tetragonal $I4_1/a$ involving a loss of symmetry elements, which causes twinning.

Radioluminescence and position of the spectral bands

Radioluminescence (RL) or X-ray induced luminescence is a sensitive technique for studying defects in minerals. X-radiation penetrates and excites the whole volume of the crystal, forming new luminescence defects. The results obtained correspond to the mean value (MV) of five replicates each, and, in all cases, the intensity of RL spectra measured for annealed samples at 1200 °C for 240 h [Fig. 3(b)] is higher than that observed for non-annealed or natural examples [Fig. 3(a)], *i.e.*, after the thermal treatment the material is more sensitive to the induced radiation. The increase in this sensitivity is due to phenomena such as (i) thermal alkali metal self-diffusion (Na and K) through the twinning interfaces of the lattice; (ii) tilting of the Al–Si crankshafts; (iii) partial phase changes; (iv) exchanges of Na^+, K^+, OH^-, H^+ and H_2O with the environment; and (v) iron redox reactions that can produce new vacancies in the lattice. The complex structure of the RL spectra for both natural and annealed leucite can be fitted with the same number of multiparameter Gaussian functions at about 300, 380, 430, 480, 560 and 680 nm and can be compared with other Na/K-aluminosilicates such as alkali metal feldspars. Thus, the UV band at 300 nm is related to defect sites associated with the presence of the content of Na in the K-aluminosilicate lattice (Table 1).[15] This peak is the most important signal in Na-rich feldspars (*e.g.*, albite) and is potentially useful for retrospective dosimetry.[16] It could, therefore, be possible to use this waveband in leucite for dosimetric purposes. Both natural and pre-heated leucites have in this emission a weaker intensity in relation to the other peaks (4.3 and 2%, respectively; Table 2). The relative intensity of this peak decreases (non-linearly) with the Na content. The thermal treatment performed on the leucite make the 300 and 380 nm intensities fade, whereas the 430 nm and green emissions increase in intensity, indicating that this peak is a thermolabile irreversible emission and is linked to the blue–green spectral zone. A similar effect has been observed in albite.[17] The relationships between spectral bands can be explained by links among defects. During the thermal self-diffusion processes the alkali metal ions most probably leak along the easier points of egress (planar defects). Conversely, atomic transport along interface–interphases destabilises the metastable equilibrium of the twin domains and unmixed phases.

The 380 nm UV emission band is characteristic of mineral phases containing SiO_4 tetrahedra (quartz and silicates) and can be related to intrinsic defects in the lattice.[17,18] This waveband is a well-studied emission and can be observed when interstitial alkali metal atoms are placed in adjacent positions to aluminium ions. Two steps are necessary to obtain this large blue emission band: (i) thermal sensitisation of the lattice with different heating time treatments and (ii) activation of emission centres under short-wavelength radiation such as X-ray, gamma or UV. The combination of the double effect observed in this leucite waveband can be described as follows: the given radiation produces mobility of the alkali metal ions causing a large number of electron–hole pairs in the lattice; some holes can be trapped, forming [AlO_4/M^+] centres. When the given energy is sufficient, recombination of the electrons with the hole trapped adjacent to Al–M^+ reduces the presence of ionic charge compensators at the Al sites and induces a 380 nm luminescence emission to [AlO_4]° centres (aluminium–hole centres). As shown in Table 2, this peak seems to be the more sensitive to thermal treatment when compared with the other peaks, since the decrease in its relative intensity is greater. Martini *et al.*[19] described a similar effect in quartz.

The relative intensity of the blue bands (at 430 and 480 nm) is the least affected by the double treatment (annealing–irradiation). The 430 nm emission (common to several feldspars with different chemical compositions and variable Al/Si order) can be attributed to recombination on a centre formed from a hole–oxygen atom adjacent to two Al atoms (Al–O–Al).[20] The 480 nm band can be assigned to the presence of Ti^{4+},[17] detected in leucite in ppm amounts. In the first case, the minor changes detected can be mainly associated with the modifications to other peaks, rather than to changes in recombination centres (Al–O–Al). The relative intensity of the lower energy band has hardly been modified owing to the very minor changes in the content of Ti^{4+} (90 ppm) which were observed.

As observed in Table 2, the green band at 560 nm is clearly affected by the thermal treatment. Unlike UV peaks, where the relative intensity decreases by more than 50%, the green band increases its relative intensity by more than 50%. This emission, common in all strain-free K-aluminosilicates, can be attributed to Mn^{2+} substitutions in calcium sites in the lattice in terrestrial and synthesised feldspars.[21] This waveband seems to be characteristic of a d^5 electronic configuration.[22] According to the chemical analysis, the content of Mn^{2+} is very low (40 ppm). This content remained unchanged from natural to annealed leucites, confirming that the irreversible 'seesaw' effect UV–

Table 1 Chemical analyses of leucite from Campania Vessa (non-annealed, annealed up to 1000 °C for 12 h and annealed up to 1200 °C for 240 h) [note the thermal alkali metal (K^+, Na^+) leakage]

	Oxide (%)									
	SiO_2	TiO_2	Al_2O_3	Fe_2O_3	MnO	MgO	CaO	Na_2O	K_2O	P_2O_5
Non-annealed	58.40	0.00	23.54	0.06	0.00	0.01	0.11	2.95	14.50	0.00
Annealed 1000 °C, 12 h	60.08	0.00	24.08	0.08	0.00	0.01	0.11	2.43	12.72	0.00
Annealed 1200 °C, 240 h	60.20	0.00	24.00	0.06	0.00	0.01	0.12	2.28	12.47	0.01

green band (decreasing–increasing) is due to the thermal treatment.

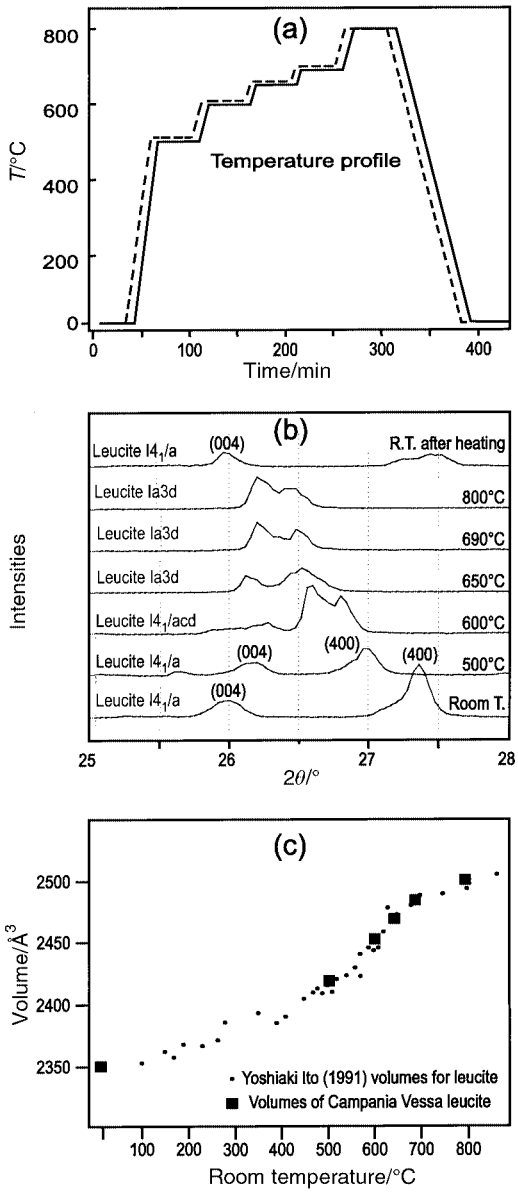

Fig. 2 High-temperature X-ray diffraction measurements of leucite. (a) Temperature profiles (time *vs.* temperature); (b) X-ray diffractogram (25–28° 2θ sector) showing the thermal evolution of (004) and (400) crystallographic planes; (c) cell volumes obtained from the refinement of crystallographic parameters by least squares. Results fitted into the plot of Ito *et al.*'s relation[13] between volume and temperature.

The red band at 680 nm, according to Kirsh and Townsend,[23] is produced when the irradiation reduces some Fe^{3+} to Fe^{2+} impurities. Iron atoms can be substituted at an Si (tetrahedrally coordinated) or an Al site in the aluminosilicate lattice, acting as recombination sites for holes or an electrons, depending on the valence. Similarly to UV radiation in K-feldspars, X-irradiation of both leucites could induce such a charge transfer between O^{2-} and Fe^{3+}.[24] The probable reaction can be described as follows:[25]

$$Fe^{3+} + e^- \rightarrow Fe^{2+} \text{ (irradiation step)}$$

$$Fe^{2+} + \text{hole}^+ \rightarrow [Fe^{3+}]^* \rightarrow Fe^{3+} + \nu \text{ (de-excitation step)}$$

The first step is a reduction process where electrons are trapped by the ferric ions, creating hole centres. In the second step, holes are trapped at hole centres by an oxidation process of ferrous ion (Fe^{2+}). In an intermediate step, the excited energy state of the Fe^{3+} is created; the following relaxation to the ground state produces the emission of a photon in the red region of the spectrum [$^4T_1(G) \rightarrow {}^6A_1(S)$ transition[26]]. As appreciated in 300 and 380 nm emissions, the red region behaves similarly after the

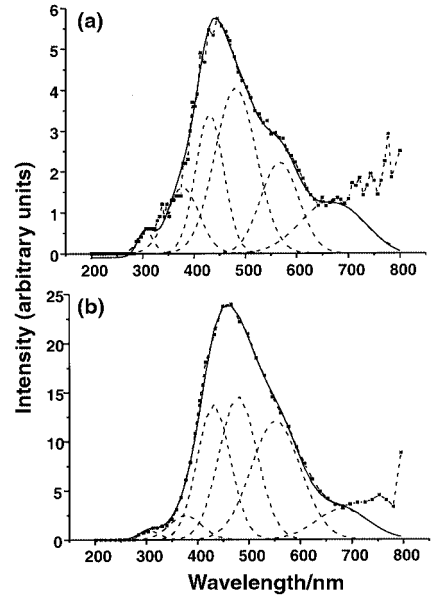

Fig. 3 Radioluminescence of the (a) non-annealed and (b) annealed (1200 °C for 240 h) leucites fitted with six multiparameter Gaussian functions. All the parameters were refined to a confidence limit of 95% accuracy. The dashed lines correspond to the calculated fitted Gaussian peaks, which make up the calculated fitted solid line. The encircling line is directly compared with the experimental dotted line that corresponds to the MV of the experimental results.

Table 2 Some physical parameters obtained from the deconvolution into Gaussian peaks of RL measurements of non-annealed and annealed (1200 °C for 240 h) leucite

	Peak No.	Position of maxima/nm	Peak energy/eV	Intensity of maxima (%)	FWHM/nm	Area of peak (%)
Non-annealed	1	305 ± 3	4.07 ± 0.04	4.3 ± 0.3	36 ± 3	1.9 ± 0.3
	2	378 ± 4	3.28 ± 0.04	12.2 ± 0.7	75 ± 6	10.9 ± 0.5
	3	430 ± 4	2.88 ± 0.03	26.0 ± 1.2	64 ± 4	19.6 ± 1.0
	4	481 ± 5	2.58 ± 0.03	30.8 ± 2.9	95 ± 5	34.5 ± 1.6
	5	567 ± 10	2.19 ± 0.04	17.0 ± 1.2	87 ± 6	17.4 ± 1.5
	6	676 ± 11	1.84 ± 0.03	9.8 ± 0.7	139 ± 12	15.7 ± 0.9
Annealed	1	306 ± 2	4.05 ± 0.03	2.0 ± 0.2	47 ± 4	1.0 ± 0.2
	2	376 ± 6	3.30 ± 0.06	5.3 ± 0.5	74 ± 5	4.3 ± 0.4
	3	432 ± 5	2.87 ± 0.03	29.4 ± 2.2	75 ± 6	24.5 ± 2.1
	4	479 ± 8	2.59 ± 0.04	31.0 ± 3.0	87 ± 6	29.7 ± 2.5
	5	553 ± 8	2.24 ± 0.03	25.7 ± 3.1	113 ± 12	32.0 ± 3.2
	6	681 ± 12	1.82 ± 0.03	6.6 ± 0.8	119 ± 14	8.6 ± 0.5

thermal treatment, *i.e.*, decreasing in relative intensity. However, the change in iron content is negligible, and therefore the variation in the relative intensity could be attributed to the sensitivity changes observed in the lattice.

Thermoluminescence

The samples (four replicates each) of natural leucite were pre-irradiated up to 20 Gy under a $^{90}Sr/Y$ β-source to monitor the glow curves in the 400 nm region and their progressive growth. Natural leucite displays a 170 °C signal, masked by a broad plateau between 100 and 200 °C, a principal emission at 250 °C and, from 300 °C onwards, a non-defined emission is visible [(Fig. 4(a)]. Above 350 °C, no significant changes are detected because of the dose effect. This behaviour can be interpreted as the starting point of ionic conductivity that is linearly correlated with electrical conductivity measurements.[9] An Italian leucite was examined by electrical conductivity methods and a contour plot was obtained including dielectric loss (tan δ) as a function of frequency and temperature, in addition to the phase transition. The authors[9] included a second resonance which started close to 300 °C and maintained its amplitude virtually constant. This is in contrast to the first peak, the resonance of which reached a minimum at the cubic–tetragonal phase transition. For these reasons, it should be possible to link the high-temperature plateau of the TL curves with Na thermal self-diffusion across the bulk and/or discontinuities of the lattice. The continuous range of small peaks of this TL glow curve fits an ionic thermal self-diffusion process or an anisotropic thermal vibration of Na atoms in the closed cell positions. These TL curves were deconvoluted to determine some physical parameters such as trap energies or pre-exponential factors. For this, both first- and second-order kinetic equations were used, but the best fit parameters obtained, based on the value of the factor of merit, were unsatisfactory. Considering the complexity of the glow curves of natural leucite, speculation about a structure of a continuous trap distribution as in other aluminosilicates involving multi-order kinetics is valid. For non-annealed leucite, the dose dependence can be fitted to a mathematical linear function of the type $y = a + bx$, where y is the intensity of the TL signal (considering the area of the curve in the range 60–500 °C), x is the given dose and a and b are constants. In the studied range, good linearity was observed ($r = 0.991$) [Fig. 4(b), Table 3].

Using the same analytical routine as for annealed leucite (12 h at 1000 °C), the shape of the glow curve, intensity and behaviour with dose change drastically when compared with natural leucite. The maximum intensity of the TL glow curve (*e.g.*, 20 Gy) increases fivefold, from 240 to 1200 a.u. [Fig. 5(a)]. The irradiated annealed leucite maintains the 250 °C signal well defined, but the most intense peak appears at 170 °C. As described for RL measurements, the thermal treatment involves a partial change in the structure producing an increase in sensitivity when irradiated. Similarly to natural leucite, the structure of the TL curve is also too complex to be well fitted. Good linearity ($r = 0.999$) was observed for the range of given doses [Fig. 5(b), Table 3].

The improvement in linearity agrees with (a) high alkali metal losses (K_2O ~12% and Na_2O ~18%) during the first thermal treatment (up to 1000 °C for 12 h), (b) the high cell volume expansion (from 2350 to 2500 Å) and (c) the tetragonal–cubic phase transition. All this would promote the egress of alkali metal ions and the production of $[AlO_4/M^+]°$, $[AlO_4/H^+]°$ and $[AlO_4]°$ luminescence centres.

Acknowledgements

We are grateful to Professor P. D. Townsend for the guidelines for the experiments and Dr. M. L. Clarke for recording the RL measurements using the high-sensitivity TL spectrometer at the

Table 3 Fitting parameters obtained from the linear function of the dose dependence of non-annealed and annealed (1000 °C for 12 h) leucite taking into account the area of the TL glow curves in the range 60–500 °C

	a	*b*	*r*
Non-annealed	11 670	841	0.991
Annealed	3 708	3 491	0.999

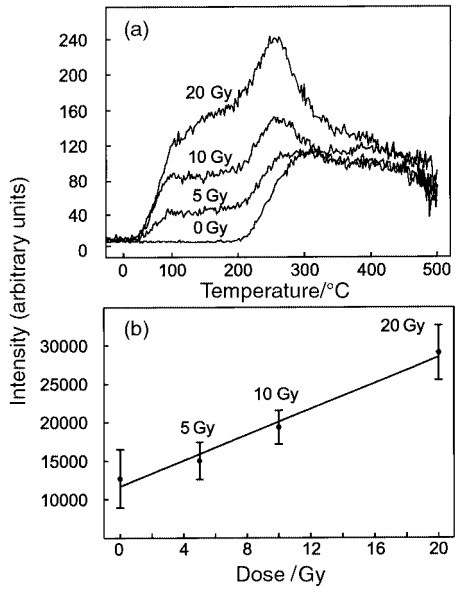

Fig. 4 (a) TL glow curves of the natural leucite from Campania Vessa (Italy). (b) Dose dependence fitted to a linear function, $y = a + bx$, where y is the intensity of the TL signal (considering the area of the curve in the range 60–500 °C), x is the given dose and a and b are constants (Table 3).

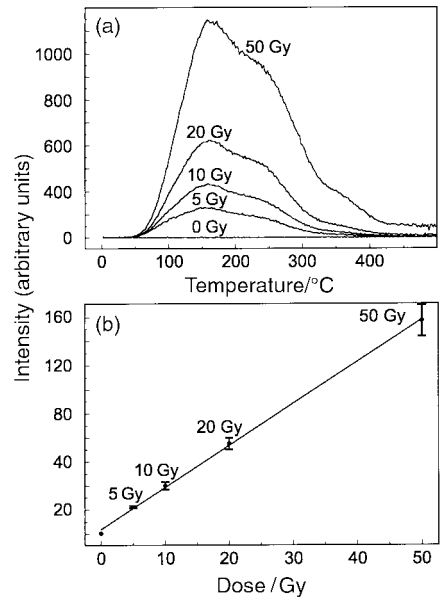

Fig. 5 (a) TL measurements of the irradiated annealed leucite (1000 °C for12 h) and (b) response to the dose fitted to a mathematical linear function of the type $y = a + bx$; good linearity ($r = 0.999$) was observed (Table 3).

University of Sussex. Thanks are due to Eladio Vila for the high-temperature X-ray measurements and Paul Giblin for a critical review of the manuscript. The work was supported by the DGICYT, project PB 98-0501.

References

1 I. Szabo, B. Nagy, G. Volksch and W. Holand, *J. Non-Cryst. Solids*, 2000, **272**(2–3), 191.
2 J. R. Mackert, Jr. and C. M. Russell, *Int. J. Prosthodont.*, 1996, **9**(3), 261.
3 I. L. Denry, J. A. Holloway and S. F. Rosenstiel, *J. Dent. Res.*, 1998, **77**(4), 583.
4 M. Martini, A. Paleari, G. Spinolo and A. Vedda, *Phys. Rev. B*, 1995, **52**(1), 138.
5 R. K. Gartia and G. B. Robertson, *Nucl. Tracks Radiat. Meas. Part D*, 1989 **16**(4), 231.
6 D. Bodoardo and M. Salis, *Nuovo Cimento Soc. Ital. Fis., D*, 1994, **16**, 403.
7 N. R. J. Poolton, L. Bøtter-Jensen and O. Johnsen, *Radiat. Meas.*, 1997, **27**(2), 279.
8 F. Mazzi, E. Galli and G. Gottardi, *Am. Mineral.*, 1976, **62**, 108.
9 D. C. Palmer, U. Bismayer and E. K. H. Salje, *Phys. Chem. Miner.*, 1990, **17**, 259.
10 G. Vantendeloo, S. Ghose and S. Amelinckx, *Phys. Chem. Miner.*, 1989, **16**(4), 311.
11 B. J. Luff and P. D. Townsend, *Meas. Sci. Technol.*, 1993, **4**, 65.
12 L. Bøtter-Jensen and G. A. T. Duller, *Nucl. Tracks Radiat. Meas.*, 1992, **20**(4), 549.
13 Y. Ito, S. Kuehner and S. Ghose, *Z. Kristallogr.*, 1991, **197**, 75.
14 D. Taylor and C. M. B. Henderson, *Am. Mineral.*, 1968, **53**, 1476.
15 J. Garcia-Guinea, H. M. Rendell and L. Sanchez-Muñoz, *Radiat. Protect. Dosim.*, 1996, **66**(1–4), 395.
16 V. Correcher, J. M. Gómez-Ros and A. Delgado, *Radiat. Protect. Dosim.*, 1999, **84**(1–4), 547.
17 M. L. Clarke and H. M. Rendell, *Radiat. Meas.*, 1997, **27**(2), 221.
18 J. Garcia-Guinea, P. D. Townsend, L. Sanchez–Muñoz and J. M. Rojo, *Phys. Chem. Miner.*, 1999, **26**, 658.
19 M. Martini, G. Spinolo, A. Vedda and C. Arena, *Solid State Commun.*, 1994, **91**(9), 751.
20 B. Speit and G. Lehmann, *J. Lumin.*, 1982, **27**, 127.
21 J. E. Geake, G. Walker, D. J. Telfer, A. H. Mills and G. F. J. Garlick, *Geochim. Cosmochim. Acta*, 1973, **3** (Suppl. 4), 3181.
22 J. R. Prescott and P. J. Fox, *J. Phys. D: Appl. Phys.*, 1993, **26**, 2245.
23 Y. Kirsh and P. D. Townsend, *Nucl. Tracks Radiat. Meas.*, 1988, **14**(1–2), 43.
24 G. H. Faye, *Can. Mineral.*, 1969, **10**, 112.
25 Y. Kirsh, *Phys. Status Solidi A*, 1991, **127**, 265.
26 N. R. J. Poolton, L. Bøtter-Jensen and O. Johnsen, *Radiat. Meas.*, 1996, **26**(1), 93.